Mon. Not. R. Astron. Soc. **260,** 241–252 (1993)

Evolution of galaxy clustering: new data on the angular correlation function of faint galaxies

Warrick J. Couch,[1] J. S. Jurcevic[1] and B. J. Boyle[2]
[1] *School of Physics, University of New South Wales, PO Box 1, Kensington, NSW 2033, Australia*
[2] *Institute of Astronomy, Madingley Road, Cambridge CB3 0HA*

Accepted 1992 June 12. Received 1992 June 4; in original form 1992 March 24

ABSTRACT

We present new results on the angular correlation function of galaxies, $w(\theta)$, and its evolution with apparent magnitude at $VR \leq 23.5$ mag. The analysis has been carried out on a data set containing 116 000 galaxies covering almost 4 deg^2 at high galactic latitudes, obtained with the Berkeley $f/1$ CCD camera on the 3.9-m Anglo–Australian Telescope. We find that, at scales less than 0°.2, $w(\theta)$ is well described by a pure power law, $w(\theta) \propto \theta^{-0.70 \pm 0.05}$, with no evidence for any systematic change in the value of the power-law index with apparent magnitude limit. The strength of clustering (as measured by the amplitude of the correlation function) is found to decrease strongly with apparent magnitude, consistent with a model in which galaxy clustering is increasing at a rate $R(z) \propto (1+z)$ with cosmic epoch. As such, this result is inconsistent with the predicted linear growth rate of structure, $R(z) \propto (1+z)^{-1}$, in the 'standard' cold dark matter model of galaxy formation.

Key words: galaxies: clustering – galaxies: formation – large-scale structure of Universe.

1 INTRODUCTION

One of the severest challenges to modern theoretical cosmology is the explanation of the formation and growth of the diverse structures (voids, filaments, clusters, superclusters) which characterize the large-scale distribution of visible matter in the Universe. Fundamental to any model which attempts to reproduce this structure (e.g., the cold dark matter model, see Davis et al. 1985) are the assumed matter content of the Universe (and, in particular, its composition) and the form of the initial perturbation spectrum from which the structure grew. Here the study of galaxy clustering at past as well as at present epochs can supply vital clues: the evolution of clustering will bear the collective imprint of all matter, visible or invisible, while the signal measured on the largest scales will strongly reflect the form of the initial power spectrum (Davis 1991).

The standard diagnostic for quantifying galaxy clustering is the two-point spatial correlation function $\xi(r)$ (Limber 1953; Groth & Peebles 1977). However, it requires a full three-dimensional specification of the galaxy distribution, thus restricting such analyses to those regions of the Universe which have been surveyed in redshift. The heavy demand such surveys place on telescope time means that a knowledge of $\xi(r)$ is, over large scales, confined to quite shallow depths (e.g., de Lapparent, Geller & Huchra 1986) and, over larger depths, is confined to small 'pencil-beam' areas of sky (Kirshner, Oemler & Schechter 1979; Bean et al. 1983).

An economical if not quite so direct approach to characterizing the galaxy distribution is to analyse it in its projected form by way of the two-point angular correlation function $w(\theta)$. While its exact relationship to $\xi(r)$ is dependent on a number of assumptions (Phillipps et al. 1978, hereafter P78; Peebles 1980), $w(\theta)$ can none the less provide useful information on clustering over a range of scales and look-back times without recourse to large amounts of telescope time. To this end, photographic surveys and, in particular, the all-sky surveys conducted on Schmidt telescopes have, with the aid of fast measuring machines, been well utilized in determining $w(\theta)$. To moderate depths ($m_B \leq 20$), at least, $w(\theta)$ has been found to be consistently described at small angular scales by a power law of the form

$$w(\theta) = A_w \theta^{-\delta},$$

with an index $\delta \approx 0.8$ and an amplitude A_w which scales reasonably well between samples of different depth (Groth & Peebles 1977; MacGillivray & Dodd 1979; Shanks et al. 1980; Hewett 1982; Collins, Heydon-Dumbleton & MacGillivray 1989; Maddox et al. 1990).

In studies that have extended this analysis to fainter depths ($m_B \sim 24$), using galaxy catalogues assembled from 4-m telescope prime-focus plates, there has not been the same level of concurrence. Koo & Szalay (1984, hereafter KS) presented correlation functions which were described by a power law with an index $\delta \approx 0.8$ to $B \sim 23$, beyond which they observed flatter slopes with $\delta \sim 0.5$. Pritchet & Infante (1986, hereafter PI) saw a similar trend with a $\delta = 0.8$ power-law slope to $B \lesssim 22.5$ and a flattening at fainter magnitudes. However, at $B > 22.5$ their amplitudes A_w were roughly twice as large as those of Koo & Szalay over the same magnitude interval. The Durham group (Stevenson et al. 1985) found no deviation from a $\delta = 0.8$ slope right down to $B_J = 24$, but saw a significant evolution in A_w with depth such that the amplitudes were a factor of ~ 2 smaller than KS's at $B_J = 24$. This was further corroborated in a later study by the same group (Jones et al. 1988) with an even stronger evolution in A_w, the effect this time being observed in the red band as well as in the blue.

Recently, a number of CCD-based studies have enabled $w(\theta)$ analyses to be performed at considerably fainter limits ($m_B \sim 26$), albeit over much smaller ($\ll 1$ deg^2) areas of sky. Efstathiou et al. (1991, hereafter E91) presented results based largely on the faint ($24 < B_J < 26$) (and predominantly blue) galaxies identified in the deep CCD survey of Tyson & Seitzer (1988). Their correlation functions, which covered scales $\theta \lesssim 0.06°$, had little or no signal, indicating an absence of clustering amongst this population. These authors concluded that either the galaxies in question constituted an extremely subluminous population of nearby objects, or galaxy clustering evolution had been far more rapid than allowed for by the standard gravitational instability theories. An analysis of CCD imagery of a 0.2-deg^2 radio–optical survey region which covered the magnitude interval $14 \lesssim V \lesssim 26$ and scales $\theta \lesssim 0.45°$ (Neuschaefer, Windhorst & Dressler 1991) showed $w(\theta)$ to have a roughly constant ($\delta = 0.6$–0.8) power-law slope over this entire range. Neuschaefer et al. found A_w to decrease monotonically with depth down to $V \sim 25$ but below this limit A_w was seen to rise again, indicating an increase in clustering strength at these very faint magnitudes. However, the data sample suffered from incompleteness and selection effects at $V > 25$, making this latter result somewhat insecure.

In this paper we present new data on the two-point angular correlation function which cast new light on the issues raised in both the faintest photographic studies and the deeper CCD work. The source of our data is a large set of frames taken with a wide-field CCD imager on the 3.9-m Anglo–Australian Telescope (AAT) as part of a search for cosmologically distant Type Ia supernovae (Couch et al. 1992; Goldhaber et al. 1992). The repeated monitoring of large (~ 4 deg^2) areas of sky to faint depths which this entails provides an ideal and, in some ways, unique data base for an analysis of $w(\theta)$. The $\sim 0.3°$ field of view of the system gives an areal coverage comparable to that of the 4-m photographic studies, and yet free of the photometric instabilities which are inherent to photographic plates. The effectively long exposures realized by the monitoring procedure ensure a depth that well exceeds that achieved in the faintest photographic studies and approaches that attained in the aforementioned CCD studies. Thus we are able readily to address the form of $w(\theta)$ over the scales and magnitudes where there was discordance among the photographic studies. We are also able to study $w(\theta)$ at depths sufficiently faint to examine the trends seen in the CCD studies.

The layout of this paper is as follows. The observations and photometric calibrations are described in Section 2, while in Section 3 we discuss the reduction procedures and techniques used in the production of the galaxy catalogue upon which our analysis is based. The details of our $w(\theta)$ analysis are given in Section 4, followed by the presentation of the results in Section 5. The results are discussed and conclusions are drawn in Sections 6 and 7, respectively.

2 OBSERVATIONS

2.1 Instrumentation

The supernova search is being carried out at the prime focus of the AAT using a focal reducer custom-built for this purpose. The focal reducer module contains a diamond-turned hyperboloidal aluminium mirror which reflects the $f/3.3$ primary beam of the telescope down through three BK-7 refractive glass elements, converting it to an $f/1$ beam with a plate scale of 50.53 arcsec mm^{-1}.

The CCD used in combination with the focal reducer is an unthinned 1024×1024 pixel THX 31156 chip manufactured by Thomson-CSF. It has 19 μm square pixels which correspond to an angular size of 0.98 arcsec and yield a total field of $0.28° \times 0.28°$. For this programme it is operated at a gain of 5 e$^-$ ADU^{-1} and a readout noise of 10 e$^-$ (rms). Being unthinned, the CCD has only red sensitivity with a detective quantum efficiency of ~ 40 per cent over the wavelength range 5000–8000 Å. Accordingly, the focal reducing optics have been designed to give optimum performance over this range.

The programme is being conducted through a single wide '*VR*' band which, effectively, is a combination of the standard *V* and Kron–Cousins *R* bands. It represents the most effective choice in terms of maximizing the detected flux from any supernova event given the wavelength dependence of both the throughput of the system and the night sky brightness. The filter element comprises a combination of the KG3 (3 mm) and GC495 (2 mm) Schott glass filters. The overall throughput of the optical system (telescope plus focal reducer plus *VR* filter) is ~ 50 per cent, except in the very corners of the field where vignetting reduces it to ~ 40 per cent.

2.2 Data collection

A number of selected regions have been set up around the sky for supernova monitoring, with the main criteria in their selection being (i) location at high galactic latitudes ($|b| > 50°$), and (ii) location away from the ecliptic plane (to avoid asteroids). Within each region, a 25-deg^2 area of sky was divided up into an 18×18 square grid of contiguous fields, each the size covered by the $f/1$ imager, to provide an initial target list. In order to avoid heavily saturating the CCD, which in the case of the Thomson device leaves remnant images which persist for up to 5 min after readout, each field was inspected visually on a red UK Schmidt Telescope sky survey plate and rejected if it contained stars brighter than $m_R \sim 12$. This led to ~ 15 per cent of the fields being retained as final targets, of which only about half were eventually observed.

The data have been acquired over two observing seasons providing repeat exposures of fields over a time baseline of several months to a year. For this study, we have used the two regions which have been most intensively monitored: the SGP (0055 − 28) region and the F249 (0340 − 45) region. A log of the observations obtained for these regions is presented in Table 1. Included are the central RA and Dec. (in 1950 coordinates) of each region (columns 2 and 3), the number of fields observed in each region (column 4), the epochs at which they were observed (column 5), the average image FWHM (as measured on the frames) experienced on each occasion (column 6), and the average airmass at which the fields were observed (column 7). The 47 observed fields, distributed in the main non-contiguously within the two regions, amount to a total sky coverage of 3.64 deg^2. The exposure time for each field was 300 s per night, the exposure being split into two consecutive 150-s integrations to provide a check on spurious images such as those caused by cosmic ray events. The majority of fields were observed at all epochs, giving overall exposures of 900 and 1500 s per field for the SGP and F249 regions, respectively. From a signal-to-noise ratio point of view, this disparity in the total exposure times is largely negated by the differences in seeing experienced for the two regions (see Table 1).

For reasons of efficiency and to expedite the supernova detection process, care was taken to obtain reasonable registration of frames between different epochs. At the beginning of each night the pointing of the telescope and the orientation of the CCD dewar were checked using the first-epoch (1989 November 30) data as a reference. This ensured that the epoch-to-epoch alignment was to within 0°.03 in rotation and 5–30 pixels in translation. This small amount of disregistration between frames had the same positive benefit as the 'on-field chopping' procedure of Tyson & Seitzer (1988), whereby the exposure of images at different physical locations on the CCD leads to the averaging out of residual effects not removed by the flat-fielding process.

2.3 Photometric calibration

A photometric calibration for the entire data set was established from the frames gathered on the night of 1990 November 13, when all the fields used in this study were observed in superb photometric conditions. The excellent quality of this night was ascertained from the repeated monitoring throughout the night of the E2 region sequence of Graham (1982). Six of the sequence stars were contained within our field; a series of aperture magnitudes was measured for each standard using the FOTO routine in the FIGARO reduction package. After making corrections for atmospheric extinction, for which we derived a primary coefficient k_{VR} of 0.17 ± 0.03 mag per airmass, the instrumental magnitudes derived for each star (using a 9-pixel diameter to give essentially 'total' magnitudes) repeated over the course of the night to better than ± 0.004 mag (rms).

To determine photometric zero-points for our non-standard VR band, a VR magnitude system had first to be defined. This we did in terms of the standard V and R bands, simply defining VR to be the average of V and R: $VR = (V+R)/2$. The VR values thus defined for the six E2

Table 1. Summary of observations.

Region	Mean RA(1950)	Mean Dec(1950)	Fields	Epochs	Average Seeing*	Average Airmass
SGP	00 27 00	-27 30 00	20	1989 Nov 30	1.8	1.14
				1989 Dec 28	1.9	1.33
				1990 Nov 13	1.9	1.02
F249	03 40 00	-45 00 00	27	1989 Nov 30	1.8	1.21
				1989 Dec 28	2.0	1.30
				1990 Jan 23	2.3	1.33
				1990 Nov 13	2.5	1.13
				1990 Nov 18	2.6	1.14

*Image FWHM as measured on data frames.

standards provided zero-points which were in consistent agreement at the ± 0.010-mag level. Within the small colour range of our standards ($0.3 < V-R < 0.6$), at least, there was no discernible evidence of any colour equation.

Given the non-standard nature of our VR band, it is useful to give a transformation between it and the standard BVR bands. From colours and magnitudes that we have computed synthetically as part of our modelling, which we describe later in this paper (Section 6), we find that, for present-day galaxies,

$$VR = V - 0.29(B-V) - 0.10. \qquad (1)$$

This transformation should provide estimates of VR to better than ± 0.02 mag. It also follows that the $V - VR = VR - R$ colour of a nearby E/S0 galaxy is ~ 0.38; a similarly nearby Sbc spiral galaxy will have a colour of ~ 0.28. At $z = 0.5$, the same galaxies have non-evolved colours of 0.80 and 0.54, respectively.

3 DATA REDUCTION

3.1 Initial processing

The CCD images were processed through the standard steps of co-addition, bias subtraction and flat-fielding. The first step was to add together each of the 150-s frame pairs, the positional stability of the AAT being so good that this required no frame registration. Bias subtraction involved evaluating a mean value for the pixels in the 'over-scan' region (first five rows) of the CCD and subtracting this value from all the pixels in the frame. This procedure was made possible by the complete absence of any structure in bias frames generated by the CCD and, of course, had the advantage of not introducing further noise into the data. The dark current of the Thomson CCD is sufficiently low (< 4 e$^-$ per pixel per 2000 s) that any attempts to remove it, given our short exposure times, were unwarranted.

For the third step a self-flat-fielding approach was taken, whereby up to 20 of the (co-added) frames taken throughout a night were used to derive a 'superflat', a frame for which each pixel value was set equal to the median evaluated for that pixel over all the frames. This was done after having first scaled the frames to the same mean value and then rejecting, from the set of values for each pixel, points which deviated by more than 2σ from the initially determined median. With there being no overlap at all between frames, the median in this case simply represents the 'sky' value. This proved to be a very successful technique for removing both the effects of vignetting and pixel-to-pixel sensitivity variations; upon division by the superflat frame our images were typically flat to better than 0.3 per cent of sky.

After this initial 'cleaning' of frames, a final stacking of the images taken of the same field at all the different epochs was performed. To determine the translational and rotational shifts required to register frames, we used the MERGE routine written as part of the Cambridge Automated Plate Measuring Machine (APM) image analysis package (Irwin 1985). This automatically went through the lists of images detected on the individual frames (see below) and found the optimum match between the two to provide an overall coordinate transformation from one frame to the other. A program called RESAMPLE, written and kindly provided by Dr M. C. B. Ashley, was then used to translate and rotate the data according to the derived transformation. The set of frames taken on 1989 November 30 was adopted as our reference for this procedure. An example of the final product of our cleaning and co-adding processes can be seen in Fig. 1; the image shown here of the F249 # 5 field represents the co-addition of frames taken at five different epochs, giving a total exposure time of 1500 s.

3.2 Image detection and photometry

Image detection and photometry were carried out from the co-added frames using the IMAGES algorithm within the APM image analysis package. This routine, like the others used here, forms the basis for the PISA image analysis routines in the STARLINK software collection. The IMAGES routine was used to apply an isophotal detection threshold to each co-added frame, identifying pixels lying more than 2σ (the rms sky noise) above the mean background level. In most cases, the 2σ level corresponded to slightly less than 1 per cent of the sky background. Images with more than three connected pixels at this level were then accepted as being real.

Aperture magnitudes within a 5-pixel (4.9 arcsec) diameter were derived from the IMAGES program for each of the detected images. This aperture size was adopted after establishing that it minimized the observed rms between the aperture magnitudes obtained for the same objects on the individual CCD frames of the same field. Overlapping images at the detection isophote were identified and corrections to their magnitudes were made using the method described by Irwin (1985).

For each field, the correction from aperture to total magnitude was determined by computing the difference

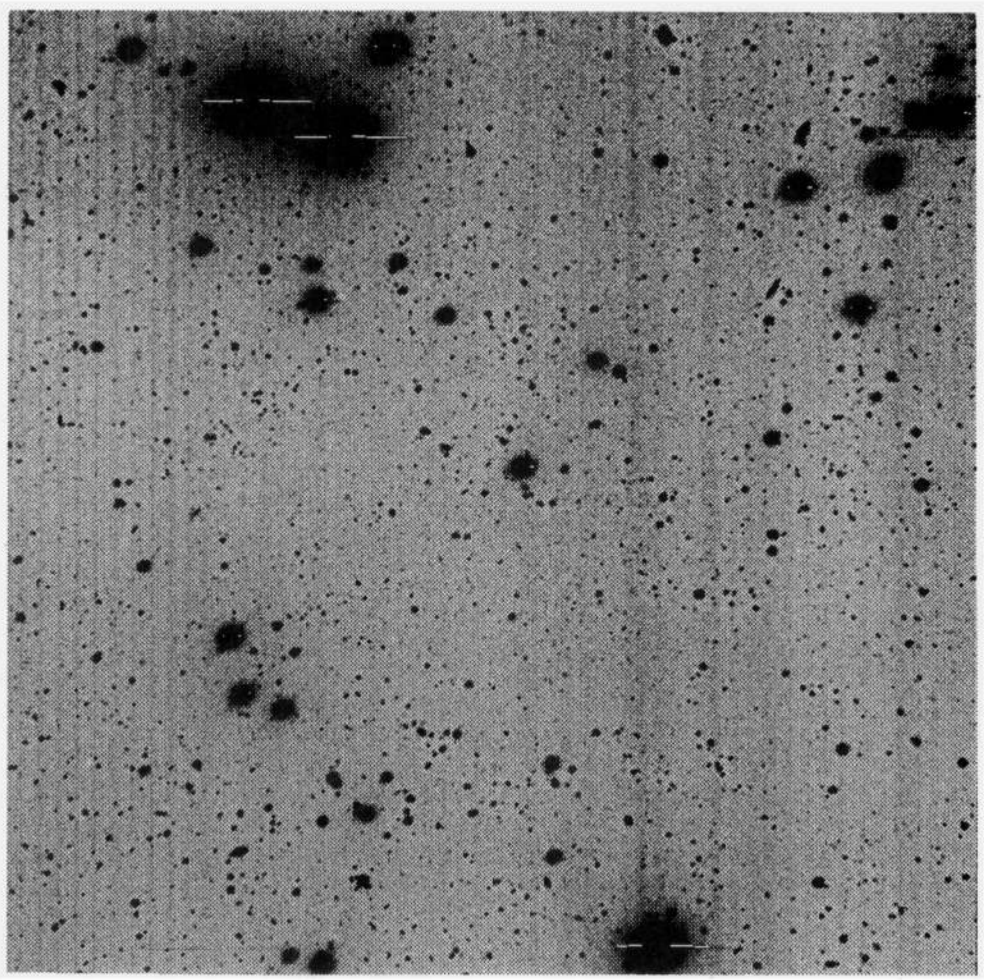

Figure 1. An example of one of our fields (F249 # 5) in its final form after frame cleaning and co-addition. It represents a total exposure of 1500 s. North is to the top, east to the left. The image is 16.7 arcmin on a side.

between magnitudes derived for 5- and 10-pixel apertures for several bright ($18 < VR < 20$) unsaturated isolated images on the co-added image. The aperture corrections derived in this manner ranged between 0.30 and 0.45 mag for the individual fields. After the aperture correction had been applied, the overall stability of the photometry from field to field was determined from a comparison of the individual number–magnitude relations for the faint images on each field. From the observed agreement between these relations, we estimate that the field-to-field photometry is accurate to ± 0.1 mag.

Classification between stars and galaxies was sought by using the STATS program in the APM image analysis package. This program utilizes a number of the parameters derived for each image in the IMAGES routine [e.g. log(area) versus magnitude] to discriminate between stellar and galaxian images. Its limitations in its application to our data are discussed in more detail below.

3.3 Production of final catalogue

In assembling a final galaxy catalogue from the lists of object positions, classifications and magnitudes produced for each field, the following 'filtering'/corrective measures were instigated.

Excision of spurious objects. Significant numbers of such objects were unfortunately produced as a result of the difficulties our detection algorithm encountered with bright ($VR < 14$) stars and with the satellite trails which appeared on several of our frames. The software had a tendency to break these features up into subimages which were sufficiently faint to enter our magnitude range of interest ($VR > 18$). For bright stars, this problem applied not just to the central peak but also to the diffraction spikes and an associated 'streak' feature produced by optical ghosting. We eliminated these spurious images from our catalogue by visually identifying the features in question (on positional plots of the images detected in each field) and, in each case, defining the smallest possible rectangular or circular excision region which enclosed all the offending objects. All the objects within these zones were then removed from the data lists; at the same time 'mask' files flagging all the pixels within these zones were produced, to be used later in constructing the random point distributions for our $w(\theta)$ analysis (see Section 4). The total area excluded in this way amounted to only a ~ 3 per cent reduction of our total sky coverage.

Star/galaxy separation. While our reduction software gave each image a 'star' or 'galaxy' classification, a visual inspection of a subset of the images on a pair of blue and red sky-limited AAT plates, which happened to overlap with some of our SGP CCD fields, indicated that this classification was not reliable at magnitudes fainter than $VR \sim 20$. This can be attributed to the large (0.96 arcsec) pixel size of our detector and the associated poor sampling of the point-spread function. Our procedure, therefore, was to remove all objects classified as stars that were brighter than $VR = 20$ and to retain all objects fainter than this limit. Our catalogue therefore suffers from some contamination by stars at $VR \geq 20$, but the contribution is small and, as far as $w(\theta)$ is concerned, can be corrected for. Exactly how small this component is can be estimated from the star count model of Bahcall & Soneira (1980, who give the integral number of stars as a function of galactic latitude and longitude, and apparent magnitude V: the fraction it predicts in the range of interest here ($20 \leq VR \leq 23.5$) is ~ 7 per cent.

Galactic absorption. Estimates of the amount of absorption present in our fields were taken from the H I-based $E(B-V)$ maps of Burstein & Heiles (1978) and Heiles & Cleary (1979). The reddening values were converted to absorption measures according to the relation $A_{VR} \simeq 2.8E(B-V)$ (Zombeck 1990), yielding A_{VR} values of 0.000 and 0.008 mag for the F249 and SGP regions, respectively. Given the small size of these estimates and the fact that they are accurate to no more than $\sim \pm 0.01$ mag, the absorption was taken to be zero for both regions and accordingly no corrections were made to our objects' magnitudes.

As a consequence of these measures, the final number of objects catalogued totalled $\sim 68\,000$ in the SGP region and $\sim 87\,000$ in the F249 region.

3.4 Counts of galaxies and completeness

Because there were differences between the airmass, the seeing and, to a lesser extent, the atmospheric transparency in which our fields (even within the same region) were observed, we expect the completeness limit of our data to vary from field to field. We judged the completeness on the basis of the number–magnitude counts in each field, using as an indicator the point at which the counts no longer continue to increase with increasing depth (for a discussion of the validity of this procedure see Kron 1980). This turnover point in the counts indicated that *all* our fields are 'complete' to $VR = 23.5$, with 15 per cent extending to $VR = 23.75$ and another 15 per cent reaching to $VR = 24$. Notably, this applies to the F249 fields and SGP fields alike, with there being no evidence that one region goes deeper than the other. To minimize the possibility of incompleteness having any bearing on our results, we have conducted our $w(\theta)$ analysis only on those objects brighter than $VR = 23.5$, where we can be confident that our samples are complete.

It is worthwhile, at this point, to compare our galaxy counts with those of other workers as a check on our data. Furthermore, the very deep counts being furnished by CCD-based studies (e.g., Tyson & Seitzer 1988; Metcalfe et al. 1991, hereafter MSFJ) are providing new and much stronger constraints on the evolutionary history of galaxies and cosmology. MSFJ have conveniently compiled a comparative plot of their counts and those derived by other workers (see their fig. 11), and we use this as our reference here. Their counts, however, are for the R_F band and so we have adjusted our VR counts on to this system. To do so, we have used the mean $VR - R_F$ colours that our models predict for the galaxies contained in the magnitude slice corresponding to each of our half-magnitude bins. The applied shift ranges from 0.35 mag at $VR = 18.25$ (appropriate to a mean redshift of 0.16) up to 0.79 mag at $VR = 23.35$ (appropriate to a mean redshift of 0.61). Note that the models incorporate the same analytical form of luminosity evolution that MSFJ found to fit their counts (see Section 6).

Our corrected counts for each of the F249 and SGP regions are plotted in Fig. 2; the dashed lines indicate the

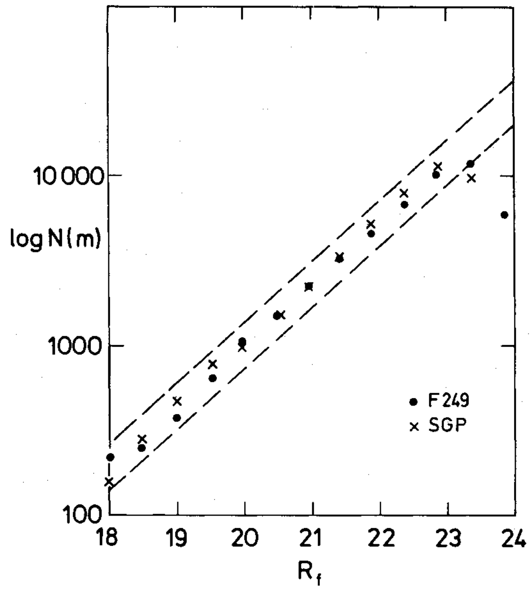

Figure 2. A comparison of our galaxy number counts with the compilation of Metcalfe et al. (1991). Our data, which are shown as the filled circles and crosses (see legend), represent the number of galaxies observed per square degree per half-magnitude interval in *VR* and transformed on to the R_F scale (abscissa). The errors in individual points are too small to be plotted in the figure. The envelope containing the various number counts presented in Metcalfe et al.'s comparison is indicated by the dashed lines.

envelopes within which the various counts in MSFJ's comparison lie. Clearly, our counts show excellent agreement with the results of these other studies in terms of both slope and absolute number. They therefore provide additional confirmation of the trends seen in the number counts at these faint limits in these other studies. Note that the turnover in our counts at $R_F \geq 23$ ($VR \sim 23.5$) is due entirely to the effects of incompleteness (see above).

4 $w(\theta)$ ANALYSIS

Our estimation of $w(\theta)$ involved the traditional method of analysing the observed galaxy distribution with reference to a random distribution generated in a Monte Carlo fashion. First, the pairing of galaxies as a function of angular separation was determined by taking each catalogued galaxy in turn and evaluating the angular separations between it and all the other galaxies in the same CCD field. Evaluating the galaxy pairs on an intrafield basis only was a restriction we imposed as a result of the signal in the correlation function at larger separations diminishing to the point where it was swamped by the field-to-field systematics in the photometric calibration. The separations were binned into 23 bins of constant $\Delta \log \theta$ covering the range $-2.5 \leq \log \theta \leq -0.3$ (11 arcsec $\leq \theta \leq 0.^\circ5$), to provide an overall summed pair distribution, $N_{gg}(\theta)$.

A similar analysis was also applied to a random point distribution. This distribution was generated by setting the number of points equal to the total number of observed galaxies and distributing them randomly over all the fields, weighting each field according to its total non-excised area (see Section 2.3). Any point which landed in an excision zone was rejected (and a new one generated again) so that the random distribution covered an area identical to that of the data.

Unlike the pair analysis for the data points, the random distribution was analysed by using each catalogued galaxy and evaluating the pairings it had with the random points in the same field. This approach is, in essence, no different from a random–random evaluation, given that the random sample will be randomly distributed with respect to the galaxy distribution, but is preferred in practice since it provides more stable estimations of $w(\theta)$ (Shanks, private communication). This was indeed verified by comparing our results with a few sample calculations based on a random–random normalization.

Finally, to minimize any noise contribution that the random point calculations might make, the galaxy–random pair evaluation was repeated 10 times, each time using a newly generated set of random points. From this a mean galaxy–random pair distribution, $\bar{N}_{gr}(\theta)$, was derived which was then combined with $N_{gg}(\theta)$ to provide our estimate of $w(\theta)$:

$$w(\theta) = 2\,\frac{N_{gg}(\theta)}{\bar{N}_{gr}(\theta)} - 1 - w_{rg}(\theta). \quad (2)$$

As prescribed by Sharp (1979) and Hewett (1982), the last term in this expression, $w_{rg}(\theta)$, is included to account for the effects of any small-amplitude large-scale gradients across the fields, as well as for $w(\theta)$ being biased by the positioning of large-scale features in the galaxy distribution with respect to the sample boundaries. It is given by

$$w_{rg}(\theta) = \frac{1}{2}\,\frac{\bar{N}_{rg}(\theta)}{\bar{N}_{rr}(\theta)} - 1, \quad (3)$$

where $\bar{N}_{rg}(\theta)$ and $\bar{N}_{rr}(\theta)$ are the summed random–galaxy and random–random pair distributions, respectively.

Another source of bias inherent to this method of estimation comes from the use of the observed number of galaxies within the sample boundaries as an estimate of the size of a randomly distributed population contained within the same boundaries. This introduces what is known as an 'integral constraint', whereby the total number of pairs in the random distribution is required to be equal to the total number of pairs in the observed distribution. Thus, if our estimate of $w(\theta)$ is positive at small separations, it will be forced to go negative at large separations. In our case the impact of this effect should be small since, in practice, the number density of random points in a given field is equal to the mean galaxy density observed over *all* fields (rather than that observed in the same field). Hence the galaxy surface density is being sampled over scales sufficiently large ($\sim 5°$) to dilute significantly the number density enhancements due to clustering. We shall examine this issue of the integral constraint further when presenting our results in the following section.

In conducting our $w(\theta)$ estimations, seven sets of calculations were each separately performed on the SGP and F249 catalogues, using different magnitude subsets of the data. To study the behaviour of $w(\theta)$ with increasing depth, analyses were carried out for the intervals $18 \leq VR \leq 21$, $18 \leq VR \leq 22$, $18 \leq VR \leq 23$ and $18 \leq VR \leq 23.5$ (hereafter referred to as the

'M18' samples). In addition, the form of $w(\theta)$ within disjoint but contiguous magnitude slices was studied, with the intervals $21 \le VR \le 22$, $22 \le VR \le 23$ and $23 \le VR \le 23.5$ (hereafter referred to as the 'MF' samples) each being individually analysed. The total number of objects from which these samples were drawn (i.e., the number contained within the interval $18 \le VR \le 23.5$) was ~53 000 for the SGP region and ~63 000 for the F249 region.

5 RESULTS

The results of our $w(\theta)$ analysis are presented in Figs 3–6. Figs 3 and 4 contain the M18 correlation functions for the SGP and F249 regions, respectively. Calculations for the MF magnitude intervals are shown in Figs 5 and 6. To aid the comparison between the correlation functions derived for the different magnitude slices, the data points have been offset in the vertical direction. In Figs 3 and 4 the data set for the $18 \le VR \le 22$ magnitude interval is plotted in its true position, while the other three sets have been shifted by integer amounts of 0.5 in log $w(\theta)$ (as clearly labelled). Similarly, in Figs 5 and 6 the $22 \le VR \le 23$ data set remains fixed while the other two correlation functions have been shifted up or down by 0.5 in log $w(\theta)$. The error bars plotted on all the points represent combined 1σ limits based on the $\sqrt{N}$ uncertainty in N_{gg} and the standard error in $\overline{N}_{gr}$ for that bin. We note that, for the 18–23 and 18–23.5 mag intervals, the sample size is such that the size of these errors for the majority of points is impressively small.

Inspection of Figs 3–6 shows that, to $\theta \sim 0^\circ.2$, at least, our galaxy samples are strongly correlated *at all depths* and our

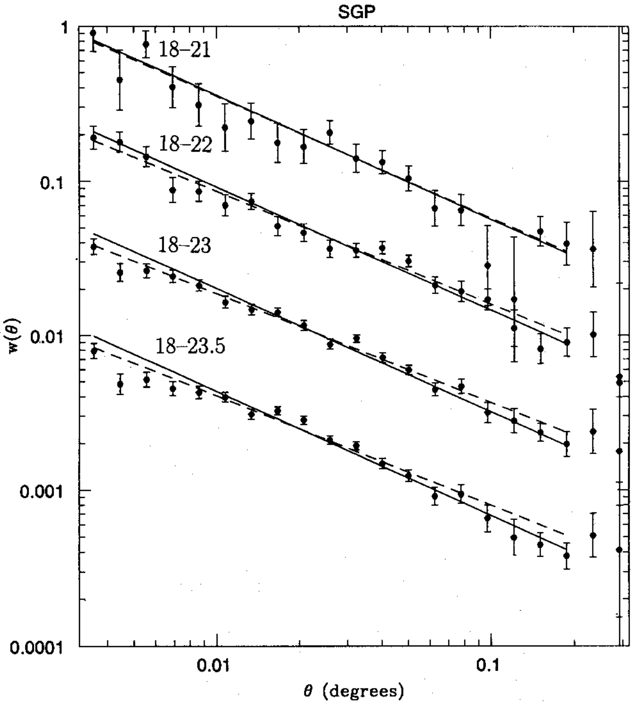

Figure 3. Correlation function estimates, $w(\theta)$, for the SGP region derived from an analysis of galaxies contained in the magnitude intervals $18 \le VR \le 21$, $18 \le VR \le 22$, $18 \le VR \le 23$ and $18 \le VR \le 23.5$. Values of $w(\theta)$ estimated for each angular bin are shown as the filled circles. The dashed lines represent linear least-squares fits through those points at $\theta \le 0^\circ.2$. The solid lines indicate a power law with index $\delta = 0.8$. Note that the '18–22' data points are plotted in their true position; the '18–21' points have been shifted upwards by +0.5 in log $w(\theta)$ and the '18–23' and '18–23.5' points have been shifted downwards by −0.5 and −1.0 in log $w(\theta)$, respectively.

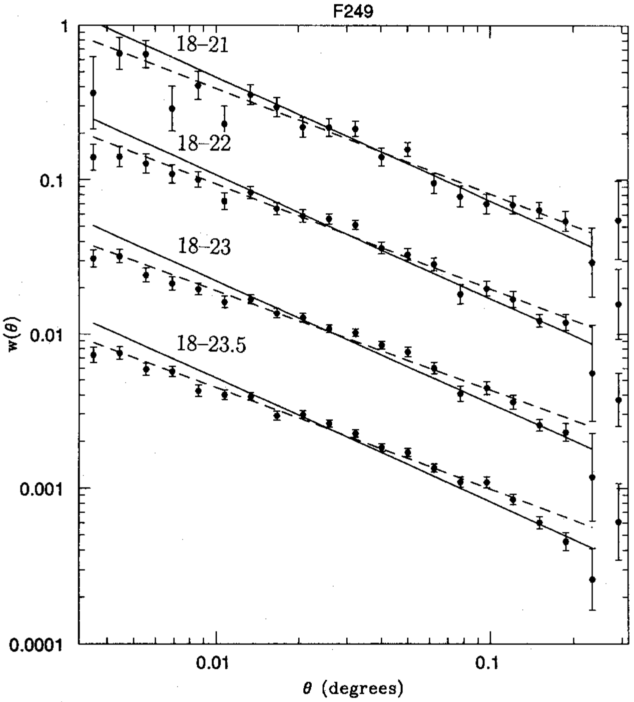

Figure 4. As Fig. 3, for the F249 region.

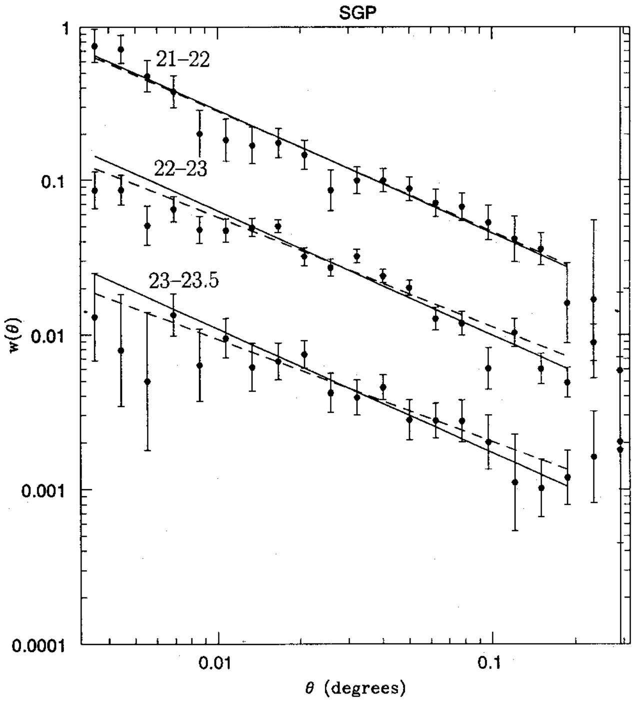

Figure 5. As Fig. 3, but for the magnitude intervals $21 \le VR \le 22$, $22 \le VR \le 23$ and $23 \le VR \le 23.5$. The '22–23' data points are plotted in their true position; the '21–22' and '23–23.5' points have been shifted +0.5 and −0.5 in log $w(\theta)$, respectively.

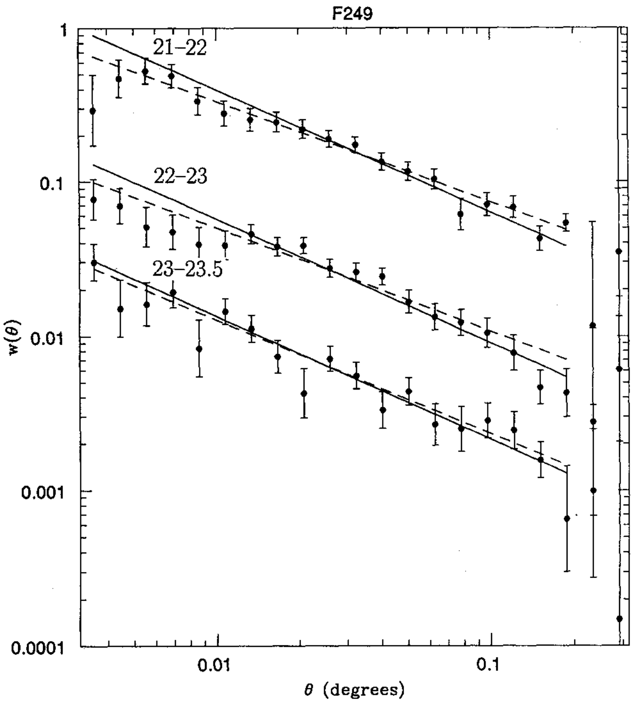

Figure 6. As Fig. 5, for the F249 region.

$w(\theta)$ estimates are consistent with a power-law behaviour (linear in the log–log plane). At $\theta > 0.^\circ 2$, the data become rapidly noisier due to the diminution in the number of pairs at these separations as the confines of our CCD field are reached. Accordingly, our attention will subsequently be restricted to the data at separations smaller than $0.^\circ 2$ deg.[1] Also notable at the largest separations is the absence of any dramatic change in the behaviour of $w(\theta)$, such as might be expected from the effects of the integral constraint (see Section 4).

Weighted linear least-squares fits made to the data in the interval $0.^\circ 003 \leq \theta \leq 0.^\circ 2$ are shown in Figs 3–6 as the dashed lines. They can be readily compared with the solid lines drawn through each set of points which indicate a power law with the canonical $\delta = 0.8$ index (see Section 1). Two qualitative conclusions can be immediately drawn from this comparison:

(i) all of the correlation functions, irrespective of the magnitude interval or the region of the sky they are from, have slopes reasonably close to the $\delta = 0.8$ value;

(ii) nowhere do we see any significant depth-dependent trends in the slope of $w(\theta)$ (cf. KS; PI).

To make a more quantitative assessment of the data, we refer to Table 2, where in column 2 we list the δ values derived from our fits. It can be seen that within a given region the value of this parameter is, to within its uncertainty, constant over all the magnitude intervals analysed. This is seen most emphatically in the M18 results for F249 (Fig. 4), where there is a range of only 0.03 in the fitted slopes (commensurate with their uncertainty). In the SGP data (M18 and MF), there is perhaps a hint of δ decreasing with increasing depth, but it is only a 1σ effect which is insignificant in comparison to the trends seen in the data of KS and PI. Evaluating a mean power-law slope for the two regions from the M18 data, we get $\bar{\delta} = 0.73 \pm 0.05$ for the SGP and $\bar{\delta} = 0.67 \pm 0.02$ for the F249 region; the difference between the two provides the most direct indication of the level at which systemic errors are present in our data. Both of the $\bar{\delta}$ values, which are representative of the data right down to their limit of $VR = 23.5$, are in consistent agreement with the 0.6–0.9 range in δ seen previously both in the brighter ($m_B \leq 20$) studies (e.g., Groth & Peebles 1977; for other references see Section 1) as well as in a subset of the fainter photographic and CCD studies (Stevenson et al. 1985; Jones et al. 1988; Neuschaefer et al. 1991; plus the brighter subsamples of KS and PI). Quite importantly, the agreement with the shallow samples also suggests that our faint sample is representative of a normal galaxy population in terms of its clustering properties.

Because the correlation function amplitude, A_w, is strongly coupled to δ, it is dangerous to base its interpretation or comparison with other studies simply on the 'raw' values obtained from the least-squares fits. To overcome this problem and achieve consistency with other studies, we have adopted the procedure of measuring A_w with δ fixed at a value of 0.8. This involves introducing an integral constraint correction factor, B, which acts as a scaling term in equation (2), which becomes

$$w(\theta) = 2\,\frac{N_{\rm gg}(\theta)}{B\bar{N}_{\rm gr}(\theta)} - 1 - w_{\rm rg}(\theta), \qquad (4)$$

in order that it provide an estimate of $w(\theta)$ with a $\delta = 0.8$ index. In practice, B was treated as a free parameter which was adjusted by trial and error until a computed correlation function with a $\delta = 0.8$ slope was obtained. The B values derived for the M18 samples are listed in column 3 of Table 2. These range from 1.0009 to 1.0208, indicating that only a very small amount (0.09–2 per cent) of scaling is required.

The extent and direction by which B deviates from unity provides a further indication of the level at which the

Table 2. Correlation function parameters.

mag. interval	δ	B	$N_{\rm obj}$	$\left(\frac{N_{\rm obj}}{N_{\rm obj}-N_s}\right)^2$	$\log A_w^{\rm corr}$
		SGP			
$18 \leq VR \leq 21$	0.78 ± 0.05	1.0009	6425	1.439	-2.40 ± 0.10
$18 \leq VR \leq 22$	0.73 ± 0.03	1.0043	15142	1.382	-2.55 ± 0.07
$18 \leq VR \leq 23$	0.70 ± 0.03	1.0052	35111	1.245	-2.79 ± 0.06
$18 \leq VR \leq 23.5$	0.70 ± 0.03	1.0067	53037	1.190	-3.02 ± 0.08
$21 \leq VR \leq 22$	0.78 ± 0.05		8717		
$22 < VR \leq 23$	0.71 ± 0.04		19969		
$23 < VR \leq 23.5$	0.66 ± 0.08		17926		
		F249			
$18 \leq VR \leq 21$	0.68 ± 0.03	1.0078	9044	1.514	-2.34 ± 0.07
$18 \leq VR \leq 22$	0.67 ± 0.02	1.0208	19974	1.429	-2.62 ± 0.11
$18 \leq VR \leq 23$	0.65 ± 0.02	1.0140	42707	1.286	-2.86 ± 0.08
$18 \leq VR \leq 23.5$	0.66 ± 0.02	1.0066	63222	1.221	-2.95 ± 0.05
$21 \leq VR \leq 22$	0.66 ± 0.04		10930		
$22 < VR \leq 23$	0.67 ± 0.05		22733		
$23 < VR \leq 23.5$	0.74 ± 0.06		20515		

[1]Note that, at the mean redshift, $\bar{z} = 0.47$, of our sample (which we determine as part of our modelling of the correlation function described in Section 6), an angular separation of $0.^\circ 2$ corresponds to a spatial separation of $2.75\,h^{-1}$ Mpc; $h = H_0/100$.

systematic effects of integral constraint and field-to-field photometric errors contribute to our $w(\theta)$ estimates. With our observed correlation functions having such small amplitudes on the largest ($\sim 0\overset{\circ}{.}2$) scales studied here, the B factor has the effect of adding or subtracting a constant offset of $(1-B)$ from $w(\theta)$ at these scales to make it match the assumed power law. In this way, the combined effects of the integral constraint (which introduces a negative offset) and field-to-field errors (which add a positive offset) are corrected for. To disentangle these two effects, we can estimate the size of the offset introduced by the integral constraint from the relation

$$\Delta w = \frac{1}{\Omega^2}\iint w(\theta_{12})\,\mathrm{d}\Omega_1\,\mathrm{d}\Omega_2 \tag{5}$$

(Groth & Peebles 1977; E91). Here the integrals are over the solid angle, Ω, of our fields. Representing $w(\theta_{12})$ by a standard $\delta = 0.8$ power law with an amplitude equal to our observed corrected values (see below), we find the B values predicted for our M18 samples to range from 0.995 to 0.9987. That these fall ~ 0.008 below our observed values can be nicely accounted for by our field-to-field photometric errors, the implied σ of ~ 0.09 mag from field to field being in close agreement with our previous estimate (see Section 3.2).

As a final step in the derivation of A_w, we correct for the diluting effects of those stars fainter than $VR = 20$ that have not been removed from our catalogues (see Section 3.3). This is done by taking the 'slope-constrained' values of the amplitude, A_w^B, and correcting them according to the relation

$$A_w^{\mathrm{corr}} = \left(\frac{N_{\mathrm{obj}}}{N_{\mathrm{obj}} - N_{\mathrm{s}}}\right)^2 A_w^B. \tag{6}$$

Here, N_{obj} (listed in column 4 of Table 2) is the total number of objects from which $w(\theta)$ was derived and N_{s} is the number of contaminating stars estimated from the model of Bahcall & Soneira (1980). The correction factor calculated from these two quantities is given in column 5 of Table 2.

The values of log A_w^{corr} are tabulated in column 6 of Table 2; they are also plotted as a function of limiting VR magnitude in Fig. 7. Reassuringly, we see that the sets of amplitudes derived independently for the SGP and F249 regions show very close agreement. We now proceed, in the following section, to examine the implications of the observed decline in amplitude with increasing depth for the evolution of galaxy clustering with cosmic epoch.

6 INTERPRETATION AND DISCUSSION

The method for modelling the observed decline in the amplitude of $w(\theta)$ with increasing sample depth (often referred to as the 'amplitude-scaling' relation) has been well developed and documented by a number of authors (e.g., Peebles 1973; P78; KS). To interpret our results, we utilized the technique detailed by P78 for dealing specifically with very deep samples in which cosmological, relativistic and evolutionary effects are important. This was facilitated by the provision of the code originally written by Dr S. Phillipps for this purpose and subsequently modified by Dr L. Jones to incorporate more up-to-date values for key parameters.

Briefly, the model is based on the fundamental assumption that the true distribution of galaxies in space is described by a spatial correlation function of the form

$$\xi(r, z) = Ch(z)\,r^{-1.8}, \tag{7}$$

where r is proper length, C is a constant and $h(z)$ is a term introduced to provide for an evolution in clustering scale with look-back time. Having specified the galaxy distribution in three dimensions, it is then a matter of integrating over the sight-lines to all the galaxies contained within the appropriate volume of space to determine the projected two-dimensional distribution and hence $w(\theta)$ (whose functional form, at least, will be a power law with index $\delta = 0.8$: Limber 1953). The most critical step in this process is accurately identifying the volume of space sampled by the data set in question.

For deep magnitude-limited samples such as ours, the determination of the associated volume limits requires a knowledge of the galaxy luminosity function and its type dependence, the relevant K-corrections and the amount of luminosity evolution galaxies have undergone with look-back time. The data we adopted can be summarized as follows.

(1) *Luminosity functions.* A Schechter (1976) function with slope parameter $\alpha = -1.25$ was used to represent each of the different galaxy types (E, S0, Sab, Scd, Sdm). Characteristic absolute magnitude values, M^*_{VR}, for each type were determined by taking the locally determined $M^*_{B_J}$ values of Peterson et al. (1986) and translating them according to the $B_J - VR$ colours computed from the nearby E/S0, Sab, Sbc, Scd and Sdm spectral energy distributions of Pence (1976). Values of the luminosity function normalization parameter Φ^* (galaxies Mpc^{-3}) for each type were also taken from Peterson et al. MSFJ have noted that Φ^* is a poorly determined parameter; however, we find our conclusions remain unchanged if the slightly larger Φ^* values determined by Kirshner et al. (1978) or Zwicky et al. (1961–68) are used.

(2) *K-corrections.* Calculations for our VR band were made for each galaxy type using the aforementioned spectral energy distributions of Pence (1976). Values were computed at intervals of 0.025 in redshift out to $z = 2.0$ and then least-squares-fitted by a second-order polynomial to provide an analytical representation.

(3) *Evolutionary corrections.* We took the amount of luminosity evolution MSFJ had to invoke to explain their blue and red galaxy number counts, interpolating between their B and R corrections (see their table 7), to provide values appropriate to our VR band. (In practice, this led to adopting evolutionary corrections very close to MSFJ's R values.)

With this information specified and h and q_0 set to 0.5 and 0.02, respectively, the computational task required was an evaluation of the integral equation (equation 15) of P78, which specifically determines A_w for the model distribution. The integration over redshift involved taking successive redshift intervals (each $\Delta z \simeq 0.01$ in width) and determining the fraction of the luminosity function of each galaxy type (and hence the number of galaxies) which is visible in that interval given the limits in apparent magnitude for each of our various samples. The integration was carried out up to the redshift at which the contribution from all types had fallen to zero (typically $z \sim 2$).

The evolution of galaxy clustering was handled in the same manner as followed by P78. The scale factor for a typical cluster, R, is assumed to vary as

$$R(z)=(1+z)^{-\beta}. \quad (8)$$

This provides for three simple evolutionary scenarios: (i) clusters expand with the Universe and $\beta=+1$ – this case describes the evolution expected in the 'standard' cold dark matter (CDM) model (Davis et al. 1985) where galaxies are clustered at the time of formation and the subsequent evolution in their clustering is dominated by the underlying dark matter; (ii) there is no evolution in clustering with $R(z)=$constant and $\beta=0$; (iii) clusters collapse at the same rate as the Universe expands, with $\beta=-1$. By invoking the conservation with redshift of the galaxy number excess within a shell centred on an arbitrary galaxy and whose radius and thickness vary according to equation (8), it can be demonstrated (P78) that the evolutionary term, $h(z)$, must be of the form

$$h(z)=(1+z)^{-\eta}, \quad (9)$$

where $\eta=1.8$, 3.0 and 4.2 for the above three cases, respectively.

We emphasize that the $\beta=+1$ ($\eta=1.8$) case only reflects the growth of clustering in the *linear* regime of the CDM models. In the non-linear regime the growth of clustering will be much faster ($-2<\beta<-1$). From fig. 17 of Davis et al. (1985), it can be seen that the non-linear evolution of the galaxy correlation function in a $q_0=0.5$ universe with strong biasing occurs at comoving scales less than 0.75 h^{-1} Mpc. This is at least a factor of 2 below the typical scales we are sampling in our study; the bulk of our signal in $w(\theta)$ originates from pairs at angular separations greater than 5 arcmin, corresponding to comoving separations of more than 1.5 h^{-1} Mpc at the mean redshift ($\bar{z}=0.47$) of our sample.

The amplitude-scaling relations computed for each of the three β values are represented by the curves in Fig. 7. It can be seen that at $VR\sim21$ the differences between the three models are insignificant in comparison to the uncertainties in our data points. However, by $VR\sim23$–23.5 the model curves have diverged significantly for our data to distinguish between them easily. Quite clearly we see that our data are most consistent with the collapsing cluster ($\beta=-1$) model, the agreement being most strongly constrained by our faintest two sets of points (18–23, 18–23.5) which deviate below the $\beta=+1$ and 0 models by more than 3σ. In addition there is perhaps some evidence that our observed amplitude-scaling relation is marginally steeper than even the $\beta=-1$ model, but we are reluctant to place any significance on this, given the simple and non-dynamical nature of our models.

Returning to the clear disagreements between the scaling relations derived by different workers at these deep limits, as outlined in Section 1, the results derived here make a valuable new contribution to this debate. Briefly, the work of KS and PI showed relations in closer agreement to the $\beta=0$ or $+1$ models, in contrast to the results of Stevenson et al. (1985) and Jones et al. (1988) which showed an evolution similar to or even stronger than that predicted by the collapsing cluster model. A direct comparison with our results is difficult, since the majority of these studies were conducted in a blue band; however, Jones et al. have published results for the red (r_F) photographic band, and we plot these as well in Fig. 7. With the caveats that we have taken their data from a ($\log A_w$, integrated count) – rather than a ($\log A_w$, limiting magnitude) – plot and the comparison is made for slightly different passbands, it is clear that our data do not support such strong evolution. Importantly, though, both our data and those of Jones et al. support a *strengthening* in clustering with cosmic epoch rather than stable clustering or a weakening in clustering as prescribed by the comoving model.

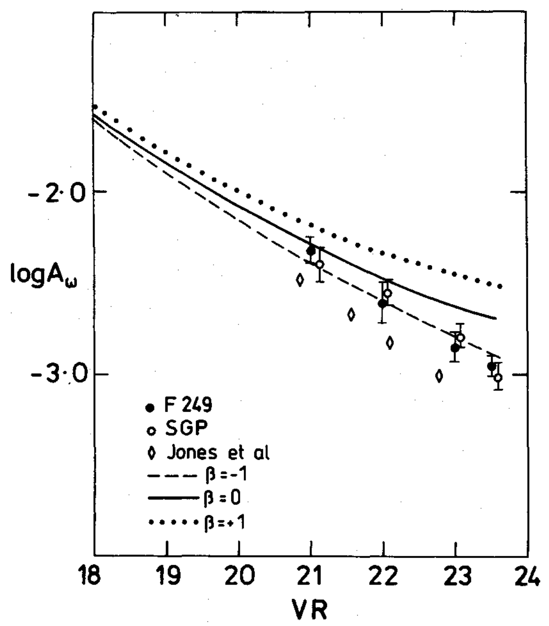

Figure 7. The observed amplitude-scaling relation plotted as a function of limiting VR magnitude. The correlation function amplitudes measured from the data presented in Figs 3 and 4 are shown as the open and filled circles (see legend for identification). The photographic-based data of Jones et al. (1988) are represented by the diamond symbols. The relations predicted from our models (see text for details) are shown as the dotted, solid and dashed curves.

Clearly, our result is also inconsistent with the linear growth of structure in a strongly biased CDM model. Indeed, the correlation function has, in the past, provided numerous observational difficulties for the predictions of the standard CDM model. The correlation function analysis of Maddox et al. (1991), based on the $B_J<20.5$ APM survey, showed $w(\theta)$ to have too much signal on large ($>20\ h^{-1}$ Mpc) scales in comparison to the CDM predictions. Similarly, in their redshift analysis of the *IRAS* sample, Saunders et al. (1991) found structure on scales too large to be explained by the CDM model. While these two studies show that the CDM scenario runs into difficulties in explaining the *present-day* distribution of galaxies, our results (as do also those of Jones et al.) show, in addition, that the rate of growth of such structure may also be inconsistent with this model. However, we concede that our observed amplitude-scaling relation may not yet prove fatal to the CDM model. For example, it may be possible to adjust the scales at which the non-linear evolution of clustering sets in, thereby driving the evolution of the correlation function at a rate much closer to that which is observed.

Finally, we examine our results in light of the very weak if insignificant clustering seen in the very faint samples analysed by E91. Their claim of little or no clustering was based primarily on a very faint blue-selected ($24\leq B_J\leq26$)

sample which cannot be directly compared with the data obtained here. However, these authors also presented results for a red-selected ($23 \leq R \leq 25$) sample drawn from the same (Tyson & Seitzer 1988) catalogue. In this case, a small but positive clustering signal was measured with a single-point estimate of $w(\theta)$ taken over the range $15 \leq \theta \leq 45$ arcsec ($\theta_{\rm eff} \sim 30$ arcsec) having a value of 0.014 ± 0.007.

Although there is only a 0.5-mag overlap between this sample and ours, and the VR and R bands are only partially matched, it is of much interest to see if this amount of signal is at all consistent with the strength of clustering seen at the faintest limits of our data. To pursue this, we extrapolated our observed amplitude-scaling relation, as well as that predicted by the $\beta = -1$ model, down to the $R = 25$ ($VR \sim 25.3$) limit of the red E91 sample. Taking the inferred value of A_w at this limit and assuming $w(\theta)$ still to be represented by a $\delta = 0.8$ power law, an estimate of $w(\theta = 30$ arcsec) was determined. This yielded values of 0.013 and 0.019 from the 'observed' and 'model' extrapolations, respectively, in very good agreement with the E91 value. Thus, while it can only be treated as an indirect indication, this result does suggest that, in the red at least, the weak level of clustering seen by E91 is not exceptional when compared with an extrapolation of the trends seen at slightly brighter limits (in particular, the observed decline in the amplitude of clustering with increasing depth).

Of course, the issue here may not be at all related to evolution in clustering, but may rather be a question of population selection. As already suggested by E91, a blue- as opposed to a red-selected sample may, at such faint limits, contain galaxy populations which are quite different. If faint samples start to be dominated by unusual and unforseen populations of objects then their observed clustering properties may well be entirely different.

In this context, the ongoing expansion of the data base upon which this study is based will be important. With the exposure of each of the fields studied here continuing to be increased, we shall eventually be able to conduct a clustering analysis at depths comparable to that of E91. With the additional benefits of large sample sizes and a broad angular coverage, it should be possible to consolidate our understanding of galaxy clustering at faint limits and, perhaps, to discriminate between evolutionary and population effects.

7 CONCLUSIONS

We have performed a two-point correlation function analysis of a complete sample of $\sim 116\,000$ galaxies catalogued within two high galactic latitude regions, covering 3.6 deg^2 and contained within the magnitude range $18 \leq VR \leq 23.5$. The salient results to emerge from our study can be summarized as follows.

(1) We have found that, over the separations studied ($\theta \leq 0\overset{\circ}{.}2$), our correlation function estimates, $w(\theta)$, exhibit a power-law behaviour to all depths within our sample.

(2) The slope index, δ, of the power-law fits to the data is found, within its uncertainty, to be invariant both with magnitude and between regions.

(3) The overall mean slope measured for our sample is $\delta = 0.70 \pm 0.05$, in agreement with that observed for the nearby normal galaxy population.

(4) Our observed amplitude-scaling relations indicate galaxy clustering to be strengthening with cosmic epoch at a rate close to that at which the Universe is expanding. The comoving picture of clustering evolution predicted by the CDM model in the linear regime is not supported by our data.

(5) An extrapolation of our results to the slightly fainter limits studied by Efstathiou et al. (1991) shows that the small degree of clustering measured by these authors in the red band, at least, may not be abnormal.

ACKNOWLEDGMENTS

We are grateful to Vikki Meadows for her assistance in the initial reduction stages. We thank the Director and staff of the Anglo-Australian Observatory for their support and help in this work. We should also like to thank Mike Irwin for providing the APM image analysis package and Simon White for useful discussions. BJB acknowledges the financial support of the Institute of Astronomy, Cambridge and the Royal Society during the course of this work. WJC acknowledges the financial support of the Australian Research Council.

REFERENCES

Bahcall J. N., Soneira R. M., 1980, ApJS, 44, 73
Bean A. J., Efstathiou G., Ellis R. S., Peterson B. A., Shanks T., 1983, MNRAS, 205, 605
Burstein D., Heiles C., 1978, ApJ, 225, 40
Collins C. A., Heydon-Dumbleton N. H., MacGillivray H. T., 1989, MNRAS, 236, 7P
Couch W. J., Perlmutter S., Newburg H. J. M., Pennypacker C., Goldhaber G., Muller R., Boyle B. J., 1992. Proc. Astron. Soc. Aust., **9**, 261
Davis M., 1991, in Latham D. W., da Costa L. A. N., eds, ASP Conf. Series Vol 15, Large-Scale Structures and Peculiar Motions in the Universe. Astron. Soc. Pacif., San Francisco, p. 379.
Davis M., Efstathiou G., Frenk C. S., White S. D. M., 1985, ApJ, 292, 371
de Lapparent V., Geller M. J., Huchra J. P., 1986. ApJ, 302, L1
Efstathiou G., Bernstein G., Katz N., Tyson J. A., Guhathakurta P., 1991, ApJ, 380, L47 (E91)
Goldhaber G., Perlmutter S., Pennypacker C., Marvin H., Muller R. A., Couch W. J., Boyle B., 1992, in Proceedings of the Supernova Watch Workshop. UCLA, in press.
Graham J. G., 1982, PASP, 94, 244
Groth E. J., Peebles P. J. E., 1977, ApJ, 217, 385
Heiles C., Cleary M. N., 1979, Aust. J. Phys. Astrophys. Suppl., No. 47, 1
Hewett P. C., 1982, MNRAS, 201, 867
Irwin M. J., 1985, MNRAS, 214, 575
Jones L. R., Shanks T., Fong R., 1988, in Bergeron J., Kunth D., Rocca-Volmerange B., Tran Thanh Van J., eds, High Redshift and Primeval Galaxies. Editions Frontières, Gif-sur-Yvette, p. 29
Kirshner R. P., Oemler R. P., Schechter P. L., 1979, AJ, 84, 951
Koo D. C., Szalay A. S., 1984, ApJ, 282, 390 (KS)
Kron R. G., 1980, ApJS, 43, 305
Limber D. N., 1953, ApJ, 117, 134
MacGillivray H. T., Dodd R. J., 1979, MNRAS, 186, 69
Maddox S. J., Sutherland W. J., Efstathiou G., Loveday J., 1990, MNRAS, 243, 692
Maddox S. J., Sutherland W. J., Efstathiou G., Loveday J., 1991, in Latham D. W., da Costa L. A. N., eds, ASP Conf. Series, Vol. 15, Large-Scale Structures and Peculiar Motions in the Universe. Astron. Soc. Pacif., San Francisco, p. 213

Metcalfe N., Shanks T., Fong R., Jones L. R., 1991, MNRAS, 249, 498 (MSFJ)
Neuschaefer L. W., Windhorst R. A., Dressler A., 1991, ApJ, 382, 32
Peebles P. J. E., 1973, ApJ, 185, 413
Peebles P. J. E., 1980, The Large Scale Structure of the Universe. Princeton Univ. Press, Princeton, NJ
Pence W., 1976, ApJ, 203, 39
Peterson B. A., Ellis R. S., Efstathiou G., Shanks T., Bean A. J., Fong R., Zen-Long Z., 1986, MNRAS, 221, 233
Phillipps S., Fong R., Ellis R. S., Fall S. M., MacGillivray H. T., 1978, MNRAS, 182, 673 (P78)
Pritchet C., Infante L., 1986, AJ, 91, 1 (PI)
Saunders W. et al., 1991, Nat, 349, 32
Schechter P., 1976, ApJ, 203, 297
Shanks T., Fong R., Ellis R. S., MacGillivray H. T., 1980, MNRAS, 192, 209
Sharp N. A., 1979, A&A, 74, 312
Stevenson P. R. F., Shanks T., Fong R., MacGillivray H. T., 1985, MNRAS, 213, 953
Tyson J. A., Seitzer P., 1988, ApJ, 335, 552
Zombeck M. V., 1990, Handbook of Space Astronomy and Astrophysics. 2nd edn, Cambridge Univ. Press, Cambridge, p. 104
Zwicky F., Herzog E., Wild P., Karpowicz M., Kowal C. T., 1961–68, Catalogue of Galaxies and Clusters of Galaxies. 6 vols, California Institute of Technology, Pasadena